ACS NANOSCIENCE Au
AN OPEN ACCESS JOURNAL OF THE AMERICAN CHEMICAL SOCIETY

pubs.acs.org/nanoau
Article

Dynamic Control of Chiral Recognition in Water-Soluble Naphthotubes Induced by Hydrostatic Pressure

Junnosuke Motoori, Tomokazu Kinoshita, Hongxin Chai, Ming-Shuang Li, Song-Meng Wang, Wei Jiang,[‖] and Gaku Fukuhara*

Cite This: ACS Nanosci. Au 2024, 4, 435−442
Read Online
ACCESS | Metrics & More | Article Recommendations | Supporting Information

ABSTRACT: The dynamic control of chiral (enantiomeric) responses in chiral host−guest complexes through external stimuli is a significant challenge in modern chemistry for developing smart stimuli-responsive materials. Herein, we report the (chir)optical properties and chiral recognition behavior of water-soluble chiral naphthotubes (**1**) under the influence of hydrostatic pressure as an external stimulus. The hydrostatic pressure spectral profiles compared to those obtained at normal pressure revealed the dynamic behavior of **1** under hydrostatic pressure, owing to the flexible linker. In chiral recognition experiments, hydrophilic amino acids such as phenylalanine (Phe) and tryptophan (Trp) exhibited reaction volume changes ($\Delta V°$) of −0.9 cm^3 mol^{-1} for D-Phe, −1.2 cm^3 mol^{-1} for L-Phe, −5.6 cm^3 mol^{-1} for D-Trp, and −7.0 cm^3 mol^{-1} for L-Trp, with enantioselectivity ranging from 1.2 to 1.6. In contrast, hydrophobic chiral styrene oxide (**2**) showed $\Delta V°$ values of 1.5 cm^3 mol^{-1} for *R*-**2** and 3.5 cm^3 mol^{-1} for *S*-**2**, with a relatively higher enantioselectivity of up to 7.6. These contrasting effects of hydrostatic pressure primarily originate from the dynamics of chiral naphthotubes.

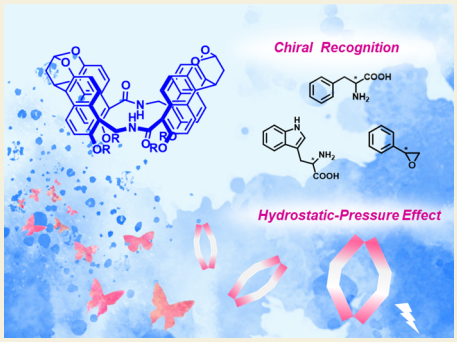

KEYWORDS: *chiral naphthotube, hydrostatic pressure, chiral recognition, enantioselectivity, dynamic control*

1. INTRODUCTION

The development of smart host molecules, such as artificial receptors and synthetic chemosensors, has garnered significant attention in multidisciplinary chemistry, particularly in the field of supramolecular chemistry.[1−6] Such smart supramolecular materials are promising candidates for potential applications in molecular memories, logic gates, and drug delivery systems.[7−9] In particular, enantiomeric responses induced by chiral guest molecule complexation are unique characteristics that can be harnessed in molecule-based devices such as 3D optical displays, security tags, and so on.[10−13] Currently, the focus is shifting toward controlling such chiral recognition responses, which is expected to lead to the development of even smarter supramolecular systems.[14−16] Therefore, in order to dynamically control chiral recognition in supramolecular complexation, a wide variety of external stimuli—such as solvent,[17−19] temperature,[20,21] electronic excitation,[22,23] and mechanical forces[24−26] (stress, strain, and pressure)—have been applied.

Recently, hydrostatic pressure or solution-state isotropic pressure has regained attention despite being an old topic, since many aspects, functions, and concepts in "mechano"-science are continually being discovered.[25] Nevertheless, mysteries remain in mechanochemical[27−29] and mechanobiological systems,[30−32] i.e., how, to what extent, and where hydrostatic pressure stimuli affect these targets. Here, we exclude high-pressure solid chemistry using a diamond anvil cell at approximately GPa,[33,34] which is beyond our target range of ca. MPa under hydrostatic pressure. Hydrostatic pressure effects in solution media have been investigated since the 1960s,[35−45] wherein some host−guest supramolecular systems under hydrostatic pressure have been examined.[46−53] However, so far, the hydrostatic pressure stimulus on chiral recognition upon supramolecular complexation has been little regarded as such a dynamic control effector. Very recently, we reported hydrostatic pressure-induced chiral responses upon the complexation of a chiral ion pair (guest) and a fluorescent anion receptor (host) with relatively effective reaction volume changes ($\Delta V°$) of 2.3−9.7 cm^3 mol^{-1}.[54] Hence, this finding encouraged us to newly explore an appreciable host-chiral guest combination that can be dynamically controlled by hydrostatic pressure. The good explanation of $\Delta V°$ in value and sign (instead of $\Delta G°$) was illustrated in the previous host−guest system.[25,47]

In this study, to dynamically control chiral responses stimulated by hydrostatic pressure, we focused on a chiral water-soluble naphthotube.[55,56] Naphthotubes are smart host molecules wherein naphthalene walls are connected by a

Received: August 26, 2024
Revised: October 7, 2024
Accepted: October 9, 2024
Published: October 21, 2024

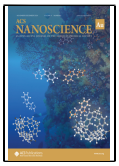

flexible methylene linker with polar functional groups.[56] Therefore, chiral naphthotubes (R^2,S^2-, and S^2,R^2-**1**, Figure 1

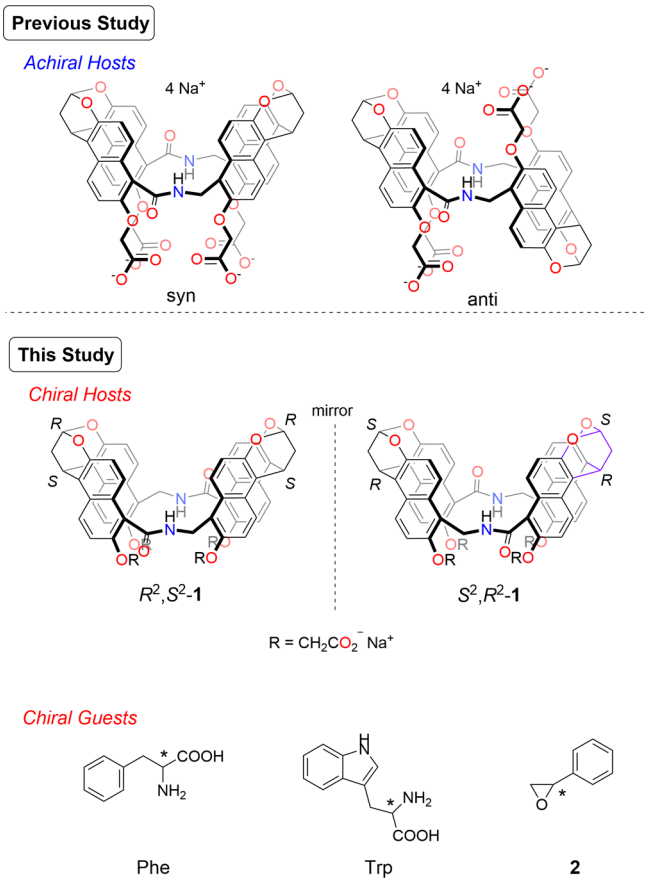

Figure 1. Chemical structures: achiral naphthotubes (top), chiral naphthotubes, and chiral guests used in this study (bottom).

(bottom))[55] provide a deeper hydrophobic cavity and a polar binding site, the combination of which plays an important role in the chiral discrimination ability in H_2O. This cooperative binding motif differs from that operative in other water-soluble chiral hosts, e.g., cyclodextrins,[57,58] chirally modified calixarenes,[59] -cucurbiturils,[60] -pillararenes,[61] and other molecular receptors.[62−66] Indeed, at an ambient pressure (0.1 MPa), the chiral naphthotube showed relatively good enantioselectivities (K_S/K_R or K_R/K_S) of up to 2.0 in H_2O when using a series of chiral styrene oxide guests.[55] More importantly, as shown in Figure 1 (top), achiral naphthotube derivatives (*anti*- and *syn*-isomers) exhibited good hydrostatic pressure effects on ΔV° as −6.3 (to *anti*) and 3.2 cm^3 mol^{-1} (to *syn*) for 1,4-dioxane.[67] These previous findings may provide us with a hint that the chiral naphthotube will function as an excellent candidate toward a pressure-responsive smart chiroptical material induced by chiral molecule complexation. Herein, we report the dynamic control of the chiral naphthotube (S^2,R^2-**1**) during chiral recognition induced by hydrostatic pressurization. For this purpose, we chose the enantiomeric pairs of phenylalanine (D/L-Phe), tryptophan (D/L-Trp), and styrene oxide (**2**) as hydrophilic guests for the former two and hydrophobic guests for the latter. The results obtained herein provide deeper insights into the factors governing the hydrostatic pressure effect of chiral naphthotubes.

2. MATERIALS AND METHODS

2.1. Materials

All commercial reagents were used as received without further purification. Fluorescence-free grade water (Milli-Q) was used for spectroscopy. Chiral naphthotubes (R^2,S^2-, and S^2,R^2-**1**) were synthesized according to a literature procedure.[55]

2.2. Instruments

The UV/vis spectra were measured by using a JASCO V-650 spectrometer. Fluorescence spectra were measured by using a JASCO FP-8500 instrument. The fluorescence lifetime decay profiles were obtained by using a Hamamatsu Quantaurus-Tau single-photon counting apparatus fitted with an LED light source. Circular dichroism (CD) spectra were obtained by using a JASCO J-720WI instrument.

2.3. Hydrostatic Pressure Spectroscopy

Spectroscopic experiments under hydrostatic pressures were conducted using a custom-built high-pressure apparatus; the details are summarized in our previous study.[25] Concisely, a quartz inner cell (2 mm path length) with a Teflon tube was filled with an H_2O solution of the sample. The cell was then placed into the outer cell, wherein sapphire windows were fitted. The tightly packed outer cell was placed in the spectrometers and hydrostatically pressurized in the range of 0.1−400 MPa. The photographs are shown in Figure S1 in the Supporting Information (SI).[25,68]

3. RESULTS AND DISCUSSION

3.1. (Chir)optical Properties and Molecular Recognition Behavior of 1

Before subjecting the compound to hydrostatic pressurization experiments, we investigated the (chir)optical properties and molecular recognition behavior of **1** in H_2O at 0.1 MPa. Although we previously measured circular dichroism (CD) spectra,[55] we did not focus on the main band in detail. Here, we report the detailed chiroptical properties of **1**. As shown in Figure 2a, at the main band based on the long axis (^1B_b transition) of the naphthalene chromophore, a strong bisignate couplet was observed in the anisotropy (g) factor profiles; $g_{239\ nm} = -0.0024$, $g_{226\ nm} = 0.0011$. According to the exciton chirality theory,[69] the observed negative exciton coupling suggests that the four naphthalene walls in S^2,R^2-**1** were aligned in a left-handed manner. In the fluorescence spectra (Figure 2b), a slightly large Stokes shift of 3280 cm^{-1} was observed despite the naphthalene chromophore, indicating excited-state flexibility or relaxation in the chiral naphthotube. As shown in Figure 2c, fluorescence lifetime decays (λ_{em}: 403, 450, and 525 nm) were reasonably fitted to a sum of two exponential functions to afford τ_1 as 0.4 and τ_2 as 3.5 ns, respectively, as listed in Table 1; all decay fitting data are shown in Figures S2−S4 in SI. By shifting the observed wavelength from 403 to 525 nm, τ_1 species was preferred (A_1: 0.81−0.94), thus indicating that the short-lived species are located in the longer wavelength region; in contrast to τ_2 at the shorter wavelength. Therefore, the longer-lived species τ_2 was ascribed to monomer-state naphthalene. In addition, the short-lived τ_1 can be assigned to the intramolecular ground-state stacked species, according to the promoted radiationless deactivation process.[70] In particular, based on the structural features observed in the X-ray single crystal,[55] this may occur in the bis(naphthalene) cleft connected by the flexible cycloalkoxy group (purple moiety in Figure 1a (bottom)); the packing structure was given in the previous report.[55] The fluorescence

https://doi.org/10.1021/acsnanoscienceau.4c00052
ACS Nanosci. Au 2024, 4, 435−442

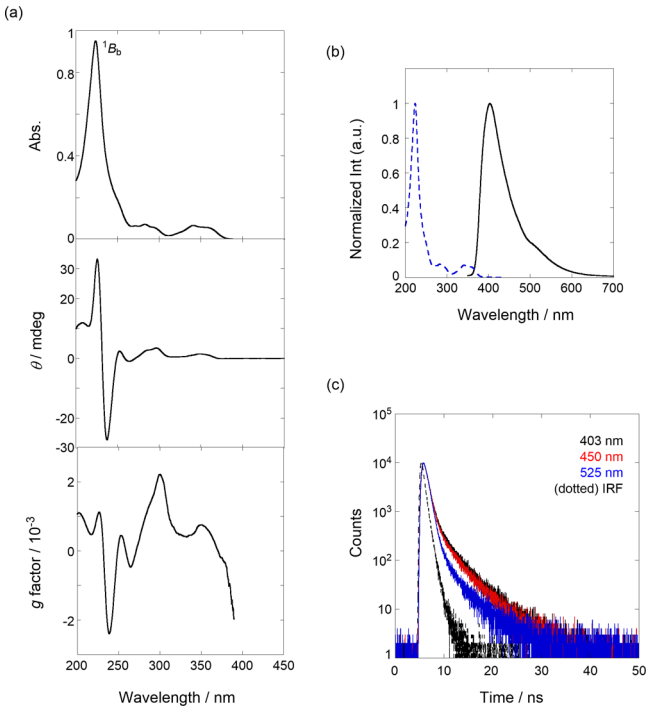

Figure 2. (a) UV/vis (top), CD (middle), and g factor spectra (bottom) of **1** (9.01 μM) in H_2O at 25 °C. (b) Fluorescence spectrum (λ_{ex}: 300 nm, black solid line) of **1** (9.01 μM) in H_2O at 25 °C; the blue dotted line represents the normalized UV/vis spectrum. (c) Fluorescence lifetime decays (λ_{ex} 280 nm) of **1** (9.01 μM), monitored at 403 (black), 450 (red), and 525 nm (blue) at room temperature. All spectra were measured in a 1 cm cell.

Table 1. Fluorescence Lifetimes of 1 in the Absence and Presence of 1,4-Dioxane in H_2O at Room Temperature[a]

compd.	λ_{em}[b] (nm)	τ_1 (ns)	A_1	τ_2 (ns)	A_2	χ^2
1[c]	403	0.4	0.81	3.5	0.19	1.3
	450	0.4	0.85	3.5	0.15	1.2
	525	0.4	0.94	3.5	0.06	1.1
1 + 1,4-dioxane[d]	403	1.6	1.00			1.3
	450	1.6[e]	0.99	3.6	0.01	1.3
	525	1.6	0.95	3.9	0.05	1.3

[a]Fluorescence lifetime (τ_i) and relative abundance (A_i) of each excited species, determined by the single-photon counting method in nondegassed solution. [b]Monitoring wavelength. [c][**1**] = 9.01 μM. [d][**1**] = 9.63 μM, [1,4-dioxane] = 5.56 mM. [e]Fixed.

quantum yield (Φ_F) was 0.07, for which the major stacked species in H_2O is highly likely responsible.

3.2. Complexation-Induced Optical Properties of 1: Dynamic Flapping

Second, we investigated the optical properties affected by the complexation of a guest molecule at 0.1 MPa. As shown in Figure 3a,b, the gradual addition of 1,4-dioxane, which was used as a guest molecule for achiral naphthotubes with a binding constant (K) of 10^3–10^4 M^{-1},[67] caused a steady increase in the fluorescence intensity, despite negligible changes in the UV/vis spectra. According to the previous binding stoichiometry,[67] Figure 3c shows the nonlinear least-squares fitting of the fluorescence titration data, assuming a 1:1 stoichiometry, which afforded K as 2930 ± 30 M^{-1}, comparable to that obtained in the achiral naphthotube. To gain deeper mechanistic insights, we measured the fluorescence lifetime decay, as shown in Figure 3d. The decay profiles with and without 1,4-dioxane were also reasonably fitted to two exponentials of τ_1 as 1.6 and τ_2 as 3.6–3.9 ns (the fitting data are shown in Figures S2 and S3 in SI). The extended τ_1 (0.4 → 1.6 ns) can be applicably accounted in terms that the intramolecular stack in the bis(naphthalene) cleft was canceled out due to the inclusion of the bulky guest. The plausible dynamic behavior of compound **1** is illustrated in Figure 3e. If the cleft works as a hinge, **1** is most likely to induce butterfly-like flapping upon guest addition. Eventually, this caused the gradual *turn-on* of fluorescence signals upon the stepwise addition of hydrophobic guests. At a host occupancy >99.9%, based on the addition of 1,4-dioxane (3.51 mM) to an H_2O solution of **1** (9.01 μM), the Φ_F value improved to 0.20, supporting the turn-on mechanism.

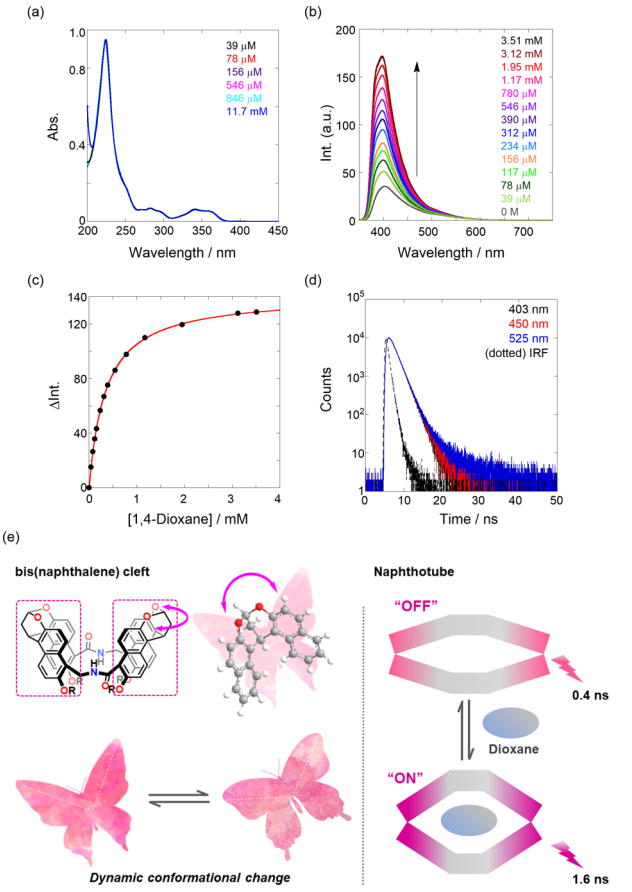

Figure 3. (a) UV/vis and (b) fluorescence spectra (λ_{ex} 300 nm) of **1** (9.01 μM) upon the addition of 1,4-dioxane (0–3.51 mM, colored lines) in H_2O at 25 °C. (c) Nonlinear least-squares fitting, assuming a 1:1 stoichiometry, to determine the binding constant (K) of 1,4-dioxane with **1**. (d) Fluorescence lifetime decays (λ_{ex} = 280 nm) of **1** (9.63 μM) and 1,4-dioxane (5.56 mM), monitored at 403 (black), 450 (red), and 525 nm (blue) at room temperature. All spectra were measured in a 1 cm cell. (e) Schematic illustration of the (*left*) dynamic flapping and (*right*) turn-on mechanism of **1**.

3.3. Hydrostatic Pressure Effects on 1

Next, we measured the hydrostatic pressure spectroscopy of **1** in the absence of chiral guests. As shown in Figure 4a, a gradual increase in absorbance upon hydrostatic pressurization was observed simply because of the increase in the effective concentration by pressurization. Interestingly, in Figure 4b, the fluorescence intensities gradually decreased, although in

https://doi.org/10.1021/acsnanoscienceau.4c00052
ACS Nanosci. Au 2024, 4, 435–442

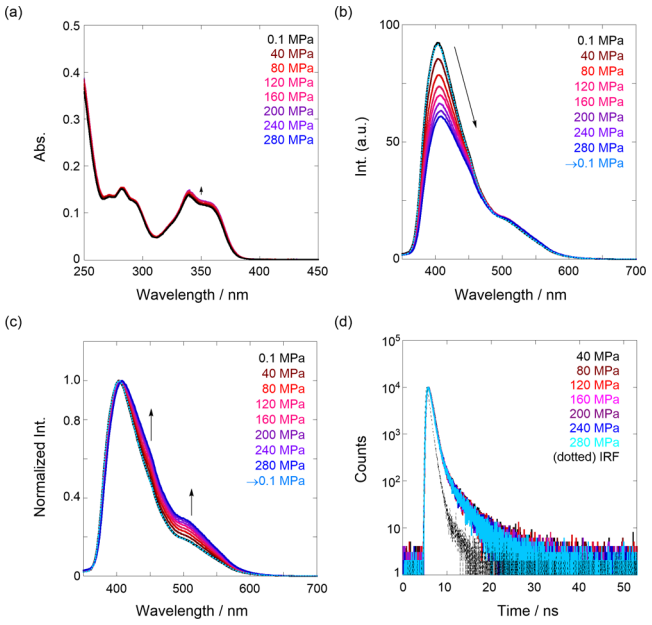

Figure 4. Pressure-dependent UV/vis (a) (90.1 μM), fluorescence (b) (9.63 μM, λ_{ex} 300 nm), normalized fluorescence spectra (c), and fluorescence lifetime decays (d) (87.9 μM, λ_{ex} 280 nm, λ_{em} 525 nm) of **1** in H_2O at room temperature over the range of 0.1−280 MPa. All spectra were measured in a high-pressure cell.

general, the intensity of fluorophores increased upon hydrostatic pressurization owing to the inhibition of solvent attack in the excited state, based on the increasing viscosity of the solution used.[45] This contrasting fluorescence behavior in **1** vs other fluorophores is well-understood by normalizing the fluorescence spectra (Figure 4c), indicating an increasing amount of intramolecular stacked species in the longer wavelength region. To confirm this further, the hydrostatic pressure lifetime decay (Figure 4d) was measured. As listed in Table 2 and Figure S4, the short-lived τ_1 was further decreased

Table 2. Fluorescence Lifetimes of 1 upon the Hydrostatic Pressurization in H_2O at Room Temperature[a]

pressure (MPa)	τ_1 (ns)	A_1	τ_2 (ns)	A_2	χ^2
40	0.42	0.93	3.2	0.07	1.1
80	0.40	0.92	3.0	0.08	1.0
120	0.39	0.92	2.8	0.08	1.2
160	0.38	0.92	2.9	0.08	1.2
200	0.36	0.90	2.4	0.10	1.3
240	0.36	0.90	2.3	0.10	0.9
280	0.35	0.90	2.3	0.10	1.1

[a]Fluorescence lifetime (τ_i) and relative abundance (A_i) of each excited species, determined by the single-photon counting method in nondegassed solution; [**1**] = 87.9 μM, λ_{em} 525 nm.

from 0.42 to 0.35 ns with increasing hydrostatic pressure, indicating that the intramolecular stacking was further promoted (more stacked). The long-lived τ_2 was also decreased from 3.2 to 2.3 ns with elevating pressure, which may be originated from gradual deactivation by pressure-induced solvent attack in the naphthalene chromophore moiety (see Figure 6c, left). Again, this suggests that **1**, particularly at the bis(naphthalene) cleft, is flexible or *dynamic* upon hydrostatic pressurization. In addition, the depressurized fluorescence spectrum (0.1 from 280 MPa (Figure 4b, sky blue line)) was superimposable on the original spectrum of 0.1 MPa (Figure 4b, black line), indicating that dynamic stacking is a reversible process.

3.4. Achiral Guest Complexation of 1 upon Hydrostatic Pressurization

For the hydrostatic pressure-binding behavior, the pressure effect of **1** upon complexation was first investigated by using achiral 1,4-dioxane. As shown in Figure S5, the gradual addition of 1,4-dioxane to an H_2O solution of **1** at different pressures (40−200 MPa) caused a steady increase in fluorescence intensity. Therefore, this "turn-on" signaling based on the guest complexation under hydrostatic pressures is most originated from the dynamic flexibility of the bis(naphthalene) cleft (stacking on/off), which is supported by the ambient and hydrostatic pressure fluorescence lifetime measurements (vide supra). Similar to the K value obtained at 0.1 MPa, nonlinear least-squares fitting of the fluorescence increase at each pressure yielded K values, as listed in Table 3. To further evaluate the hydrostatic pressure effect of **1** upon complexation more quantitatively, we calculated ΔV° according to eq 1:

$$\left(\frac{\partial \ln K}{\partial P}\right) = -\frac{\Delta V^\circ}{RT} \quad (1)$$

As shown in Figure 5, the natural logarithm of each K value obtained for 1,4-dioxane was plotted against pressure with a good linear relationship (r = 0.903), indicating that a single mechanism operated in the range of pressures studied. The ΔV° value obtained from the slope in the plot was 1.2 ± 0.3 cm^3 mol^{-1}, which is relatively small but positive. This is highly likely preferable for the tighter stacking of flexible naphthalene walls rather than the complexation-induced extension of the walls, resulting in a slight inhibition of supramolecular complexation upon hydrostatic pressurization. Therefore, the value and sign of ΔV° can provide us with the degree of dynamism in the naphthotube skeleton.

3.5. Amino Acids Complexation of 1 upon Hydrostatic Pressurization

Next, we investigated the hydrostatic pressure effects on **1** by using chiral guests. First, hydrophilic enantiomeric pairs (D/L) of Phe and Trp were investigated in a similar manner. In Figures S6 and S7, a similar trend for the complexation of Phe is observed, enabling the formation of K at each pressure (see Table 3). The enantioselectivity (K_L/K_D) of Phe ranged from 1.3 to 1.6, suggesting that the diastereomeric energy difference (**1** ⊂ D or L-Phe) had little effect on hydrostatic pressure stimulation. Interestingly, the obtained ΔV° values in the ln$K$-P plot (Figure 6a) were −0.9 ± 0.6 for D and −1.2 ± 0.2 cm^3 mol^{-1} for L, which are relatively small and similar to those of 1,4-dioxane, but negative. This behavior can be reasonably explained by the preferential opening of the flexible naphthalene walls, causing a slight promotion of supramolecular complexation stimulated by hydrostatic pressure. This is most likely because the desolvation of H_2O molecules around the hydrophilic functional groups (COO^- and NH_3^+) in Phe occurred upon complexation, leading to a decrease of ΔV° (negative sign), as illustrated in Figure 6c. A similar investigation of hydrophilic Trp provided stronger evidence of the dynamic behavior in naphthotubes. The routine hydrostatic pressure fluorescence titration of Trp (Figures S8 and S9) exhibited similar turn-on signaling to afford K_D and K_L at each pressure; the enantioselectivity varied in the range of 1.2−

https://doi.org/10.1021/acsnanoscienceau.4c00052
ACS Nanosci. Au 2024, 4, 435−442

Table 3. Binding Constants (K), Enantioselectivity, and Reaction Volume Changes ($\Delta V°$) for 1:1 Complexation of Achiral and Chiral Guests with 1 in H_2O under Hydrostatic Pressure at Room Temperature[a]

guest	pressure (MPa)	K[b] (M^{-1})	K_L/K_D K_S/K_R	$\Delta V°$ (cm^3 mol^{-1})
1,4-dioxane	0.1	2902 ± 245	[c]	1.2 ± 0.3
	40	2924 ± 213		
	80	2739 ± 230		
	120	2699 ± 237		
	160	2662 ± 241		
	200	2675 ± 267		
L-Phe	40	260 ± 20	1.5	−1.2 ± 0.2
	80	253 ± 21	1.3	
	120	264 ± 15	1.4	
	160	271 ± 21	1.5	
	200	277 ± 23	1.6	
	240	276 ± 25	1.3	
	280	289 ± 25	1.5	
D-Phe	40	178 ± 15	[c]	−0.9 ± 0.6
	80	189 ± 19		
	120	191 ± 21		
	160	186 ± 16		
	200	178 ± 22		
	240	210 ± 26		
	280	193 ± 30		
L-Trp	40	1241 ± 141	1.2	−7.0 ± 0.3
	80	1364 ± 115	1.2	
	120	1610 ± 119	1.2	
	160	1828 ± 146	1.3	
	200	1943 ± 94	1.2	
	240	2189 ± 168	1.3	
	280	2435 ± 180	1.4	
D-Trp	40	1016 ± 223	[c]	−5.6 ± 0.5
	80	1164 ± 266		
	120	1367 ± 281		
	160	1428 ± 293		
	200	1568 ± 327		
	240	1637 ± 344		
	280	1795 ± 370		
S-**2**	40	12877 ± 991	6.8	3.5 ± 0.5
	80	13618 ± 1142	7.6	
	120	12168 ± 944	6.7	
	160	12044 ± 1256	7.2	
	200	10878 ± 1541	6.4	
	240	10159 ± 1555	6.2	
	280	9649 ± 1553	5.9	
R-**2**	40	1903 ± 348	[c]	1.5 ± 0.3
	80	1786 ± 315		
	120	1812 ± 330		
	160	1673 ± 259		
	200	1689 ± 365		
	240	1648 ± 368		
	280	1648 ± 424		

[a]All titration experiments were performed in a high-pressure cell. [b]For convenience, we reported values to the nearest whole number for the ln$K$-P plots. [c]Not applicable.

1.4 (see Table 3). More importantly, the ln$K$-P plot (Figure 6b) gave $\Delta V°$ as −5.6 ± 0.5 cm^3 mol^{-1} for D and −7.0 ± 0.3 cm^3 mol^{-1} for L, the larger value of which indicates the more dynamic open-up of the naphthalene walls upon hydrostatic pressurization. As is the case with Phe, this can be reasonably explained in terms of the much greater desolvation of hydrated H_2O around the larger hydrophilic Trp moiety than that of Phe, which is most likely the origin.

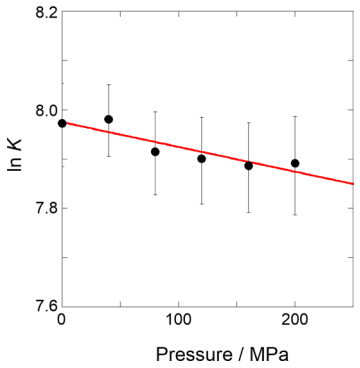

Figure 5. Pressure dependence of the binding constant (K) upon the complexation of 1,4-dioxane with **1** in H_2O under hydrostatic pressures (0.1−200 MPa) at room temperature (correlation coefficient r = 0.903).

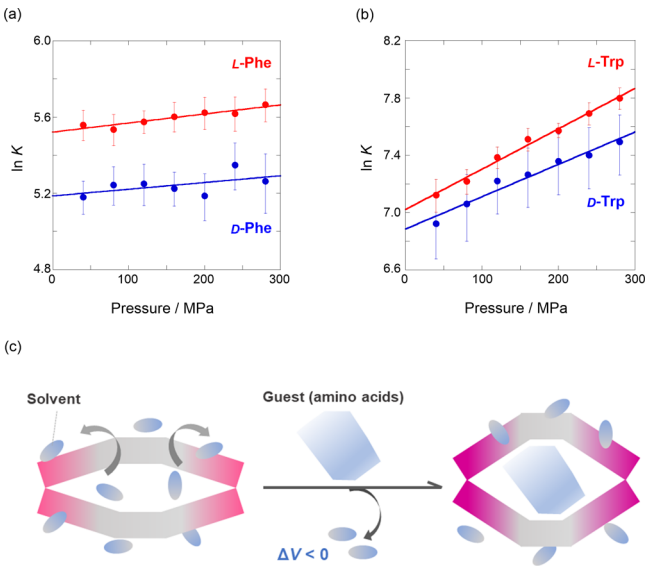

Figure 6. Pressure dependence of the binding constant (K) upon the complexation of (a) Phe (r = 0.541 for D, r = 0.938 for L) and (b) Trp (r = 0.981 for D, r = 0.995 for L) with **1** in H_2O in a hydrostatic pressure range of 40−280 MPa at room temperature. (c) Schematic illustration of the dynamic stretch of **1** stimulated by guest inclusion upon hydrostatic pressurization.

3.6. Hydrophobic Chiral Guest Complexation of 1 upon Hydrostatic Pressurization: Toward Higher Enantioselectivity

Finally, the extent to which the hydrophobic chiral guest (**2**) affected the dynamics of the naphthotube was investigated. A similar trend was observed when **2** was added to an H_2O solution of **1** under high pressure (Figures S10 and S11, Table 3). Interestingly, the addition of the *S* enantiomer showed a larger turn-on signal in the lower concentration range than the *R* enantiomer, indicating stronger binding of the *S* enantiomer. Surprisingly, the enantioselectivity (K_S/K_R) varied in the range of 5.9−7.6, which is significantly higher than those obtained in other previous chiral hosts.[57−66] This improved enantioselectivity, compared to that observed with hydrophilic amino acids,

https://doi.org/10.1021/acsnanoscienceau.4c00052
ACS Nanosci. Au 2024, 4, 435−442

may be attributed to the dynamic naphthotube tightly conforming to the size and shape of the hydrophobic guest in an induced-fit manner. This was further supported by the ΔV° values obtained from the ln*K*-*P* plot: 3.5 ± 0.5 cm^3 mol^{-1} for *S* (Figure 7a) and 1.5 ± 0.3 cm^3 mol^{-1} for *R* (Figure 7b).

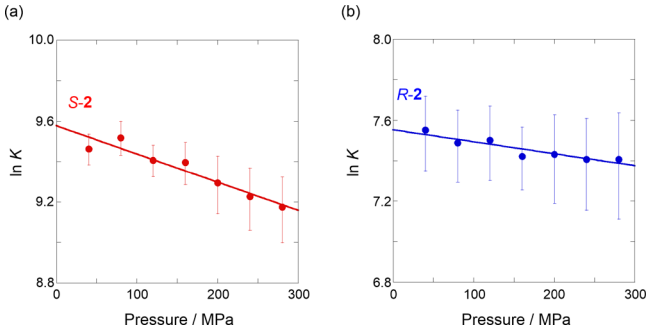

Figure 7. Pressure dependence of the binding constant (*K*) upon the complexation of (a) *S*-**2** (r = 0.955) and (b) *R*-**2** (r = 0.918) with **1** in H_2O in a hydrostatic pressure range of 40−280 MPa at room temperature.

Based on the characteristics of the dynamic naphthotube, the positive ΔV° can be easily explained by the strong solvation around hydrophobic guest **2**, which promotes the closing of the naphthalene walls. In other words, both **2** and the solvated H_2O molecules strongly bind to the cavity in the naphthotubes, suggesting that such cosolvation plays a critical role in achieving higher chiral discrimination in a dynamic chiral host.

4. CONCLUSIONS

In conclusion, we demonstrated hydrostatic pressure-induced chiral recognition of both hydrophilic and hydrophobic guests using water-soluble chiral naphthotubes. The chiral naphthotube used in this study was relatively flexible and dynamic upon hydrostatic pressure stimulation due to its flexible linker. This dynamism critically determines the contrasting complexation of hydrophilic amino acids (negative ΔV°) and hydrophobic **2** (positive ΔV°), with the desolvation/solvation of water likely playing a significant role. Notably, a high enantioselectivity of up to 7.6 was achievable using a hydrostatic pressure control approach. Hence, this study provides valuable guidelines for the development of smart chiral chemosensors, materials, and devices.

■ ASSOCIATED CONTENT

Supporting Information

The Supporting Information is available free of charge at https://pubs.acs.org/doi/10.1021/acsnanoscienceau.4c00052.

Hydrostatic pressure apparatus, fluorescence lifetime decays, and titration data (DOCX)

■ AUTHOR INFORMATION

Corresponding Author

Gaku Fukuhara − *Department of Chemistry, Tokyo Institute of Technology, Tokyo 152-8551, Japan;* orcid.org/0000-0002-2189-8943; Email: gaku@chem.titech.ac.jp

Authors

Junnosuke Motoori − *Department of Chemistry, Tokyo Institute of Technology, Tokyo 152-8551, Japan*

Tomokazu Kinoshita − *Department of Chemistry, Tokyo Institute of Technology, Tokyo 152-8551, Japan*

Hongxin Chai − *Shenzhen Xinhua Middle School, Shenzhen 518109, China*

Ming-Shuang Li − *Department of Chemistry, Southern University of Science and Technology, Shenzhen 518055, China*

Song-Meng Wang − *Department of Chemistry, Southern University of Science and Technology, Shenzhen 518055, China*

Wei Jiang − *Department of Chemistry, Southern University of Science and Technology, Shenzhen 518055, China;* orcid.org/0000-0001-7683-5811

Complete contact information is available at: https://pubs.acs.org/10.1021/acsnanoscienceau.4c00052

Author Contributions

[‖]This paper is dedicated to Prof. Wei Jiang, who passed away during this research. CRediT: **Junnosuke Motoori** data curation, formal analysis, investigation, writing - original draft, writing - review & editing; **Tomokazu Kinoshita** data curation, formal analysis, investigation, writing - original draft, writing - review & editing; **Hongxin Chai** investigation, writing - original draft, writing - review & editing; **Ming-Shuang Li** data curation, formal analysis, investigation, writing - original draft, writing - review & editing; **Song-Meng Wang** data curation, formal analysis, investigation, writing - original draft, writing - review & editing; **Wei Jiang** conceptualization, resources; **Gaku Fukuhara** conceptualization, data curation, formal analysis, funding acquisition, project administration, supervision, validation, writing - original draft, writing - review & editing.

Notes

The authors declare no competing financial interest.

■ ACKNOWLEDGMENTS

G.F. appreciates the generous support provided by Grants-in-Aid (Nos. 23H04020 and 24K01536) from the Japan Society for the Promotion of Science (JSPS) and Ajinomoto Co., Inc.

■ REFERENCES

(1) Shinkai, S.; Ikeda, M.; Sugasaki, A.; Takeuchi, M. Positive Allosteric Systems Designed on Dynamic Supramolecular Scaffolds: Toward Switching and Amplification of Guest Affinity and Selectivity. *Acc. Chem. Res.* **2001**, *34*, 494−503.

(2) You, L.; Zha, D.; Anslyn, E. V. Recent Advances in Supramolecular Analytical Chemistry Using Optical Sensing. *Chem. Rev.* **2015**, *115*, 7840−7892.

(3) Schroeder, V.; Savagatrup, S.; He, M.; Lin, S.; Swager, T. M. Carbon Nanotube Chemical Sensors. *Chem. Rev.* **2019**, *119*, 599−663.

(4) Fukuhara, G. Analytical supramolecular chemistry: Colorimetric and fluorimetric chemosensors. *J. Photochem. Photobiol. C: Photochem. Rev.* **2020**, *42*, No. 100340.

(5) Rivera-Tarazona, L. K.; Campbell, Z. T.; Ware, T. H. Stimuli-responsive engineered living materials. *Soft Matter* **2021**, *17*, 785−809.

(6) Hua, B.; Shao, L.; Li, M.; Liang, H.; Huang, F. Macrocycle-Based Solid-State Supramolecular Polymers. *Acc. Chem. Res.* **2022**, *55*, 1025−1034.

(7) *Molecular Memory and Processing Devices in Solution and on Surfaces*; Shipway, A. N.; Karz, E.; Willner, I.; Springer-Verlag: Berlin Heidelberg, 2001.
(8) de Silva, A. P.; Gunaratne, H. Q. N.; McCoy, C. P. A molecular photoionic AND gate based on fluorescent signalling. *Nature* **1993**, *364*, 42−44.
(9) Yang, J.; Wang, X.; Wang, B.; Park, K.; Wooley, K.; Zhang, S. Challenging the fundamental conjectures in nanoparticle drug delivery for chemotherapy treatment of solid cancers. *Adv. Drug Delivery Rev.* **2022**, *190*, No. 114525.
(10) Pu, L. Fluorescence of Organic Molecules in Chiral Recognition. *Chem. Rev.* **2004**, *104*, 1687−1716.
(11) David, A. H. G.; Casares, R.; Cuerva, J. M.; Campaña, A. G.; Blanco, V. A [2]Rotaxane-Based Circularly Polarized Luminescence Switch. *J. Am. Chem. Soc.* **2019**, *141*, 18064−18074.
(12) Zhan, X.; Xu, F.-F.; Zhou, Z.; Yan, Y.; Yao, J.; Zhao, Y. S. 3D Laser Displays Based on Circularly Polarized Lasing from Cholesteric Liquid Crystal Arrays. *Adv. Mater.* **2021**, *33*, 2104418.
(13) MacKenzie, L. E.; Pal, R. Circularly polarized lanthanide luminescence for advanced security inks. *Nat. Rev. Chem.* **2021**, *5*, 109−124.
(14) Shen, J.; Okamoto, Y. Efficient Separation of Enantiomers Using Stereoregular Chiral Polymers. *Chem. Rev.* **2016**, *116*, 1094−1138.
(15) Zhang, L.; Wang, H.-X.; Li, S.; Liu, M. Supramolecular chiroptical switches. *Chem. Soc. Rev.* **2020**, *49*, 9095−9120.
(16) Zhang, C.; Zhao, S.; Zhang, M.-M.; Li, B.; Dong, X.-Y.; Zang, S.-Q. Emergent induced circularly polarized luminescence in host-guest crystalline porous assemblies. *Coord. Chem. Rev.* **2024**, *514*, No. 215859.
(17) Fujiki, M. Supramolecular Chirality: Solvent Chirality Transfer in Molecular Chemistry and Polymer Chemistry. *Symmetry* **2014**, *6*, 677−703.
(18) Yashima, E.; Ousaka, N.; Taura, D.; Shimomura, K.; Ikai, T.; Maeda, K. Supramolecular Helical Systems: Helical Assemblies of Small Molecules, Foldamers, and Polymers with Chiral Amplification and Their Functions. *Chem. Rev.* **2016**, *116*, 13752−13990.
(19) García, F.; Gómez, R.; Sánchez, L. Chiral supramolecular polymers. *Chem. Soc. Rev.* **2023**, *52*, 7524−7548.
(20) Kulkarni, C.; Meijer, E. W.; Palmans, A. R. A. Cooperativity Scale: A Structure-Mechanism Correlation in the Self-Assembly of Benzene-1,3,5-tricarboxamides. *Acc. Chem. Res.* **2017**, *50*, 1928−1936.
(21) Hecht, M.; Würthner, F. Supramolecularly Engineered J-Aggregates Based on Perylene Bisimide Dyes. *Acc. Chem. Res.* **2021**, *54*, 642−653.
(22) Vallavoju, N.; Sivaguru, J. Supramolecular photocatalysis: combining confinement and non-covalent interactions to control light initiated reactions. *Chem. Soc. Rev.* **2014**, *43*, 4084−4101.
(23) Ji, J.; Wei, X.; Wu, W.; Yang, C. Asymmetric Photoreactions in Supramolecular Assemblies. *Acc. Chem. Res.* **2023**, *56*, 1896−1907.
(24) Zhou, X.; Fang, S.; Leng, X.; Liu, Z.; Baughman, R. H. The Power of Fiber Twist. *Acc. Chem. Res.* **2021**, *54*, 2624−2636.
(25) Mizuno, H.; Fukuhara, G. Solution-State Hydrostatic Pressure Chemistry: Application to Molecular, Supramolecular, Polymer, and Biological Systems. *Acc. Chem. Res.* **2022**, *55*, 1748−1762.
(26) Goldup, S. M. The End of the Beginning of Mechanical Stereochemistry. *Acc. Chem. Res.* **2024**, *57*, 1696−1708.
(27) Sagara, Y.; Kato, T. Mechanically induced luminescence changes in molecular assemblies. *Nat. Chem.* **2009**, *1*, 605−610.
(28) Pucci, A.; Bizzarri, R.; Ruggeri, G. Polymer composites with smart optical properties. *Soft Matter* **2011**, *7*, 3689−3700.
(29) Xue, P.; Ding, J.; Wang, P.; Lu, R. Recent progress in the mechanochromism of phosphorescent organic molecules and metal complexes. *J. Mater. Chem. C* **2016**, *4*, 6688−6706.
(30) Meersman, F.; Dobson, C. M.; Heremans, K. Protein unfolding, amyloid fibril formation and configurational energy landscapes under high pressure conditions. *Chem. Soc. Rev.* **2006**, *35*, 908−917.
(31) Murthy, S. E.; Dubin, A. E.; Patapoutian, A. Piezos thrive under pressure: mechanically activated ion channels in health and disease. *Nat. Rev. Mol. Cell Biol.* **2017**, *18*, 771−783.
(32) Mohammed, D.; Versaevel, M.; Bruyère, C.; Alaimo, L.; Luciano, M.; Vercruysse, E.; Procès, A.; Gabriele, S. Innovative Tools for Mechanobiology: Unraveling Outside-In and Inside-Out Mechanotransduction. *Front. Bioeng. Biotechnol.* **2019**, *7*, 162−179.
(33) Lee, R.; Howard, J. A. K.; Probert, M. R.; Steed, J. W. Structure of Organic Solids at Low Temperature and High Pressure. *Chem. Soc. Rev.* **2014**, *43*, 4300−4311.
(34) O'Bannon, E. F., III; Jenei, Z.; Cynn, H.; Lipp, M. J.; Jeffries, J. R. Contributed Review: Culet Diameter and the Achievable Pressure of a Diamond Anvil Cell: Implications for the Upper Pressure Limit of a Diamond Anvil Cell. *Rev. Sci. Instrum.* **2018**, *89*, 111501.
(35) Bovey, F. A.; Yanari, S. S. Effect of Solvent Polarizability on the Ultra-Violet Spectral Shifts of Aromatic Compounds. *Nature* **1960**, *186*, 1042−1044.
(36) Johnson, P. C.; Offen, H. W. Effect of Pressure on Pyrene Excimer Fluorescence in Toluene. *J. Chem. Phys.* **1972**, *56*, 1638−1642.
(37) Rollinson, A. M.; Drickamer, H. G. High Pressure Study of Luminescence from Intramolecular CT Compounds. *J. Chem. Phys.* **1980**, *73*, 5981−5996.
(38) Hara, K.; Yano, H. High-Pressure Study on Intramolecular Excimer Formation of 1,3-Di-1-pyrenylpropane in Various Solvents. *J. Am. Chem. Soc.* **1988**, *110*, 1911−1915.
(39) Hara, K.; Rettig, W. Effect of Pressure on the Fluorescence of TICT States in (*N*,*N*-Dimethylamino)benzonitrile and Its Related Compounds. *J. Phys. Chem.* **1992**, *96*, 8307−8309.
(40) Rettig, W.; Gilabert, E.; Rullière, C. Pressure Dependence of Bicimer Formation in 4-Dimethylamino-4'-cyanostilbene and Model Compounds. *Chem. Phys. Lett.* **1994**, *229*, 127−133.
(41) Asano, T.; Furuta, H.; Sumi, H. "Two-Step" Mechanism in Single-Step Isomerizations. Kinetics in Highly Viscous Liquid Phase. *J. Am. Chem. Soc.* **1994**, *116*, 5545−5550.
(42) Hara, K.; Kometani, N.; Kajimoto, O. High-Pressure Studies on the Excited-State Intramolecular Charge Transfer of 4-(*N*,*N*-Dimethylamino)triphenylphosphine in Alcohols. *J. Phys. Chem.* **1996**, *100*, 1488−1493.
(43) Ruan, K.; Tian, S.; Lange, R.; Balny, C. Pressure Effects on Tryptophan and Its Derivatives. *Biochem. Biophys. Res. Commun.* **2000**, *269*, 681−686.
(44) Hablot, D.; Ziessel, R.; Alamiry, M. A. H.; Bahraidah, E.; Harriman, A. Nanomechanical Properties of Molecular-Scale Bridges as Visualised by Intramolecular Electronic Energy Transfer. *Chem. Sci.* **2013**, *4*, 444−453.
(45) Suhina, T.; Weber, B.; Carpentier, C. E.; Lorincz, K.; Schall, P.; Bonn, D.; Brouwer, A. M. Fluorescence Microscopy Visualization of Contacts Between Objects. *Angew. Chem., Int. Ed.* **2015**, *54*, 3688−3691.
(46) Weber, G.; Tanaka, F.; Okamoto, B. Y.; Drickamer, H. G. The Effect of Pressure on the Molecular Complex of Isoalloxazine and Adenine. *Proc. Natl. Acad. Sci. U.S.A.* **1974**, *71*, 1264−1266.
(47) Letcher, T. M.; Mercer-Chalmers, J. D.; Kay, R. L. Volume changes in complex formation between crown ethers of cryptand-222 and alkali metals in various solvents. *Pure. Appl. Chem.* **1994**, *66*, 419−427.
(48) Isaacs, N. S.; Nichols, P. J.; Raston, C. L.; Sandova, C. A.; Young, D. J. Solution volume studies of a deep cavity inclusion complex of C_{60}: [*p*-benzylcalix[5]arene ⊂ C_{60}]. *Chem. Commun.* **1997**, 1839−1997.
(49) Ariga, K.; Terasaka, Y.; Sakai, D.; Tsuji, H.; Kikuchi, J. Piezoluminescence Based on Molecular Recognition by Dynamic Cavity Array of Steroid Cyclophanes at the Air-Water Interface. *J. Am. Chem. Soc.* **2000**, *122*, 7835−7836.
(50) Saudan, C.; Dunand, F. A.; Abou-Hamdan, A.; Bugnon, P.; Lye, P. G.; Lincoln, S. F.; Merbach, A. E. A Model for Sequential Threading of α-Cyclodextrin onto a Guest: A Complete Thermody-

https://doi.org/10.1021/acsnanoscienceau.4c00052
ACS Nanosci. Au 2024, 4, 435−442

namic and Kinetic Study in Water. *J. Am. Chem. Soc.* **2001**, *123*, 10290−10298.
(51) Ruloff, R.; Seelbach, U. P.; Merbach, A. E.; Klärner, F.-G. Molecular tweezers as synthetic receptors: the effect of pressure and temperature on the formation of host-guest complexes. *J. Phys. Org. Chem.* **2002**, *15*, 189−196.
(52) Yang, C.; Nakamura, A.; Fukuhara, G.; Origane, Y.; Mori, T.; Wada, T.; Inoue, Y. Pressure and Temperature-Controlled Enantiodifferentiating [4 + 4] Photocyclodimerization of 2-Anthracenecarboxylate Mediated by Secondary Face- and Skeleton-Modified γ-Cyclodextrins. *J. Org. Chem.* **2006**, *71*, 3126−3136.
(53) Yao, J.; Mizuno, H.; Xiao, C.; Wu, W.; Inoue, Y.; Yang, C.; Fukuhara, G. Pressure-driven, solvation-directed planar chirality switching of cyclophano-pillar[5]arenes (molecular universal joints). *Chem. Sci.* **2021**, *12*, 4361−4366.
(54) Kinoshita, T.; Haketa, Y.; Maeda, H.; Fukuhara, G. Ground- and excited-state dynamic control of an anion receptor by hydrostatic pressure. *Chem. Sci.* **2021**, *12*, 6691−6698.
(55) Chai, H.; Chen, Z.; Wang, S.-H.; Quan, M.; Yang, L.-P.; Ke, H.; Jiang, W. Enantioselective Recognition of Neutral Molecules in Water by a Pair of Chiral Biomimetic Macrocyclic Receptors. *CCS Chem.* **2020**, *2*, 440−452.
(56) Yang, L.-P.; Wang, X.; Yao, H.; Jiang, W. Naphthotubes: Macrocyclic Hosts with a Biomimetic Cavity Feature. *Acc. Chem. Res.* **2020**, *53*, 198−208.
(57) Rekharsky, M. V.; Inoue, Y. Complexation Thermodynamics of Cyclodextrins. *Chem. Rev.* **1998**, *98*, 1875−1917.
(58) Crini, G. Review: A History of Cyclodextrins. *Chem. Rev.* **2014**, *114*, 10940−10975.
(59) Sansone, F.; Barboso, S.; Casnati, A.; Sciotto, D.; Ungaro, R. A New Chiral *Rigid Cone* Water Soluble Peptidocalix[4]arene and Its Inclusion Complexes with α-Amino Acids and Aromatic Ammonium Cations. *Tetrahedron Lett.* **1999**, *40*, 4741−4744.
(60) Dai, L.; Wu, W.; Liang, W.; Chen, W.; Yu, X.; Ji, J.; Xiao, C.; Yang, C. Enhanced chiral recognition by γ-cyclodextrin-cucurbit[6]-uril-cowheeled [4]pseudorotaxanes. *Chem. Commun.* **2018**, *54*, 2643−2646.
(61) Chen, Y.; Fu, L.; Sun, B.; Qian, C.; Pangannaya, S.; Zhu, H.; Ma, J.; Jiang, J.; Ni, Z.; Wang, R.; Lu, X.; Wang, L. Selection of Planar Chiral Conformations between Pillar[5,6]arenes Induced by Amino Acid Derivatives in Aqueous Media. *Chem.—Eur. J.* **2021**, *27*, 5890−5896.
(62) James, T. D.; Sandanayake, K. R. A. S.; Shinkai, S. Chiral discrimination of monosaccharides using a fluorescent molecular sensor. *Nature* **1995**, *374*, 345−347.
(63) Singh, H.; Warmuth, R. Chiral recognition by hemicarcerand-like host in aqueous solution. *Tetrahedron* **2002**, *58*, 1257−1264.
(64) Bouchet, A.; Brotin, T.; Linares, M.; Ågren, H.; Cavagnat, D.; Buffeteau, T. Enantioselective Complexation of Chiral Propylene Oxide by an Enantiopure Water-Soluble Cryptophane. *J. Org. Chem.* **2011**, *76*, 4178−4181.
(65) Wang, B.-Y.; Stojanović, S.; Turner, D. A.; Young, T. L.; Hadad, C. M.; Badjić, J. D. The Entrapment of Chiral Guests with Gated Baskets: Can a Kinetic Discrimination of Enantiomers Be Governed through Gating? *Chem.—Eur. J.* **2013**, *19*, 4767−4775.
(66) Ríos, P.; Mooibroek, T. J.; Carter, T. S.; Williams, C.; Wilson, M. R.; Crump, M. P.; Davis, A. P. Enantioselective carbohydrate recognition by synthetic lectins in water. *Chem. Sci.* **2017**, *8*, 4056−4061.
(67) Li, S.; Yao, H.; Kameda, T.; Jiang, W.; Kitahara, R. Volumetric Properties for the Binding of 1,4-Dioxane to Amide Naphthotubes in Water. *J. Phys. Chem. B* **2020**, *124*, 9175−9181.
(68) Mizuno, H.; Kitamatsu, M.; Imai, Y.; Fukuhara, G. Smart Fluorescence Materials that Are Controllable by Hydrostatic Pressure: Peptide-Pyrene Conjugates. *ChemPhotoChem* **2020**, *4*, 502−507.
(69) Berova, N.; Bari, L. D.; Pescitelli, G. Application of electronic circular dichroism in configurational and conformational analysis of organic compounds. *Chem. Soc. Rev.* **2007**, *36*, 914−931.
(70) Vuorimaa, E.; Ikonen, M.; Lemmetyinen, H. Photophysics of rhodamine dimers in Langmuir-Blodgett films. *Chem. Phys.* **1994**, *188*, 289−302.

https://doi.org/10.1021/acsnanoscienceau.4c00052
ACS Nanosci. Au 2024, 4, 435−442